Structural Basis for Thermostability in Aporubredoxins from *Pyrococcus furiosus* and *Clostridium pasteurianum*†

Edward R. Zartler,‡ Francis E. Jenney, Jr.,§ Mark Terrell,‡ Marly K. Eidsness,|| Michael W. W. Adams,§ and James H. Prestegard*,‡

Complex Carbohydrate Research Center, Department of Biochemistry and Molecular Biology, and Department of Chemistry, University of Georgia, Athens, Georgia 30602

Received November 22, 2000; Revised Manuscript Received March 29, 2001

ABSTRACT: The structures of apo- and holorubredoxins from *Pyrococcus furiosus* (PfRd) and *Clostridium pasteurianum* (CpRd) have been investigated and compared using residual dipolar couplings to probe the origin of thermostability. In the native, metal (Fe or Zn) containing form, both proteins can maintain native structure at very high temperatures (>70 °C) for extended periods of time. Significant changes in either structure or backbone dynamics between 25 and 70 °C are not apparent for either protein. A kinetic difference with respect to metal loss is observed as in previous studies, but the extreme stability of both proteins in the presence of metal makes thermodynamic differences difficult to monitor. In the absence of metal, however, a largely reversible thermal denaturation can be monitored, and a comparison of the two apoproteins can offer insights into the origin of stability. Below denaturation temperatures apo-PfRd is found to have a structure nearly identical to that of the native holo form, except immediately adjacent to the metal binding site. In contrast, apo-CpRd is found to have a structure distinctly different from that of its holo form at low temperatures. This structure is rapidly lost upon heating, unfolding at approximately 40 °C. A PfRd mutant with the hydrophobic core mutated to match that of CpRd shows no change in thermostability in the metal-free state. A metal-free chimera with residues 1−15 of CpRd and the remaining 38 residues of PfRd is severely destabilized and is unfolded at 25 °C. Hence, the hydrophobic core does not seem to be the key determinant of thermostability; instead, data point to the hydrogen bond network centered on the first 15 residues or the interaction of these 15 residues with other parts of the protein as a possible contributor to the thermostability.

Detailed studies of the mechanisms of hyperthermostability in proteins have been dominated by the study of small proteins from archaea, most notably through studies of the redox protein rubredoxin from *Pyrococcus furiosus* (Pf)[1] and its mesophilic homologue from *Clostridium pasteurianum* (Cp). Rubredoxin is a 53−54 residue, globular protein that contains a four cysteine−iron center. The native protein from *Pyrococcus furiosus* is extraordinarily stable, maintaining native structure for hours at temperatures above 100 °C; the native protein from *C. pasteurianum* denatures more quickly. The two proteins have 78% primary sequence homology (Figure 1). Since differences are found both near the metal coordinating cysteines and elsewhere in the protein, the difference in thermostability might be expected to arise from the metal coordination, from the protein structure, or from a combination of the two. The small size (∼6 kDa) coupled with the fact that paramagnetic iron can be substituted with diamagnetic zinc with no detectable change in structure makes the proteins amenable to solution NMR studies. We employ NMR methods here to investigate the origin of thermostability.

There has been a plethora of studies focusing on the metal site of both the mesophilic and thermophilic rubredoxins using NMR, MCD, EXAFS, high-level calculations, and voltammetry (*1*−*6*), but few differences are found. There is an NMR structure of PfZnRd (*7*) and several X-ray structures of PfRd and CpRd that have been analyzed in detail (*8*−*10*). Comparison of the structures of PfRd and CpRd near the metal site reveals nothing strikingly different; the backbone atoms of the two structures have a 0.5 Å RMSD. If the metal sites are so nearly identical in the two rubredoxins, then a focus on the underlying protein structure would seem more appropriate.

A difficulty in systematic investigations of the thermodynamic origin of stability in rubredoxin is that, in the presence of metal, denaturation is irreversible. Cavagnero

† This work was supported by Grant MCB 9726341 from the National Science Foundation (E.R.Z., M.T., and J.H.P.), a National Science Foundation Research Training Grant Award to the Center for Metalloenzyme Studies (DIR 90-14281) (M.K.E.), and Grant BES-0004257 from the National Science Foundation (F.E.J. and M.W.W.A.).

* To whom correspondence should be addressed. Phone: 706-542-6281. Fax: 706-542-6281. E-mail: jpresteg@ccrc.uga.edu.

‡ Complex Carbohydrate Research Center.

§ Department of Biochemistry and Molecular Biology.

|| Department of Chemistry.

[1] Abbreviations: Pf, *Pyrococcus furiosus*; Cp, *Clostridium pasteurianum*; Rd, rubredoxin; NMR, nuclear magnetic resonance spectroscopy; MCD, magnetic circular dichroism; EXAFS, extended X-ray absorption fine structure spectroscopy; RMSD, root-mean-square deviation; TCA, trichloroacetic acid; β-ME, β-mercaptoethanol; GuHCl, guanidine hydrochloride; K-P_i, potassium phosphate; HSQC, heteronuclear single-quantum coherence spectroscopy; NOESY, nuclear Overhauser effect spectroscopy; TOCSY, total correlation spectroscopy; ANS, 1-anilinonaphthalene-8-sulfonate sodium salt.

10.1021/bi0026831 CCC: $20.00
Published on Web 05/25/2001

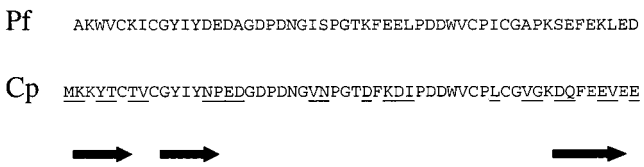

FIGURE 1: Sequence alignment of *P. furiosus* and *C. pasteurianum* rubredoxin. Underlined residues are those which are different in CpRd. Dark arrows indicate the location of the β-strands.

et al. (*11*−*13*) have studied the kinetics of unfolding of PfRd and CpRd under conditions which allow transient observation of some intermediates including ones in which the metal has been lost. This work was, however, conducted at pH 2.0 in order to eliminate electrostatic contributions to unfolding and speed up metal loss to experimentally amenable time scales. There is also some evidence from circular dichroism that the demetalated state of both CpRd and PfRd maintained some secondary structure for a number of hours at high temperature after metal loss at pH 7.8−8.2 (*13*, *14*). More recently, Mayo and Strop engineered a Pf rubredoxin that had no metal binding site (*15*, *16*). This protein was thermostable (T_m = 82 °C) but not nearly as stable as the parent PfRd (T_m > 200 °C) (*17*). This metal-free rubredoxin can be reversibly unfolded and provided the first access to thermodynamic studies of apo-like rubredoxin.

To the best of our knowledge, no systematic attempts to structurally characterize the apo forms of the native proteins have been made at high or low temperatures under aerobic or anaerobic conditions. Here we probe structures of these forms under aerobic conditions and compare them to the metalated forms using a relatively new source of structural data, residual dipolar couplings collected on the $^{15}N-^{1}H$ directly bonded pairs that are observable in NMR−HSQC spectra of the isotopically labeled proteins.

In typical solution NMR spectroscopy, dipolar couplings are seldom observed because averaging over an isotropic orientational distribution reduces the dipolar couplings between proximate pairs of magnetic nuclei to zero. However, the recent development of liquid crystalline media that impart a small degree of alignment to biological samples has allowed the measurement of dipolar couplings in solution (*18*, *19*). Dipolar couplings have been widely utilized in refining solution structures but are also very useful in studying the departure from known structures through either conformational changes or moderate amplitude internal motions (*20*). These latter analyses combine a hypothetical structure with an order matrix description of motional averaging to back-calculate dipolar couplings for comparison to the experimental values (*21*, *22*). Plotting calculated dipolar couplings against the experimentally measured values yields a well-defined straight line of unit slope when there is no departure from the proposed structure. Deviations from the line indicate the presence of motion or modification of the structure itself. We have very good structures for the native Pf and Cp rubredoxins, and the measurement of residual dipolar couplings allows efficient screening of changes prior to denaturation of the native state, with or without a substituted diamagnetic metal (Zn). Moreover, the $^{1}H-^{15}N$ HSQC spectra on which the residual dipolar coupling measurements are based provide efficient monitors of thermal denaturation through the substantial chemical shift changes upon destruction of native structure.

The initial studies of the native apo and metalated species will be extended through comparative studies to two variants. One variant involves the substitution of residues found in the distinct hydrophobic core in PfRd for those found in the CpRd core. The other involves the substitution of the first 15 residues of Pf for those found in Cp (*14*). There is a unique network of hydrogen bonds and salt bridges in PfRd centered on the side chain of E15. In CpRd this residue is a proline, a residue incapable of supporting this hydrogen-bonding network. These two chimeras will allow some delineation of the origin of any differences in the thermostability of the apo forms of native Pf and Cp rubredoxin.

EXPERIMENTAL PROCEDURES

PfZnRd, PfFeRd, CpZnRd, CpFeRd, PfRd (W3Y/I23V/L32I), and Cp15PfRd were prepared as previously described (*14*, *23*). Three forms of PfRd are produced when expressed in *Escherichia coli*, the "wild-type", N-terminal Met, and N-terminal formyl-Met forms. There is a slight difference in the thermostability of these three forms (*9*), but it is not significant in the context of our studies. Also, except for minor differences in cross-peaks from the N-terminal residues, the HSQC spectra are identical for the three forms. Nevertheless, the three forms were separated, and only one form was used for each study: wild-type for diamagnetically substituted protein and fMet-PfFeRd for paramagnetic studies. The Cp rubredoxins and the Cp15Pf chimera are expressed largely in the N-terminal Met form and were used as such.

Apo Pf and Cp rubredoxins were prepared by taking either ZnRd or FeRd and adding 1 volume of 50% TCA with 143 mM β-ME. This was mixed vigorously and then pelleted by centrifugation. This was done three times. The resultant white pellet of demetalated protein was resuspended in 5 M GuHCl/143 mM β-ME and dialyzed extensively against 1.1× PfRd buffer (55 mM K-P_i, 220 mM NaCl, 143 mM β-ME, pH 6.5) or 1.1× CpRd buffer (165 mM Na_2SO_4, 110 mM Na-P_i, 143 mM β-ME, pH 7.0) for apo-PfRd and apo-CpRd, respectively. The metal content was analyzed by inductively coupled argon plasma spectroscopy (ICAP) at the Chemical Analysis Facility (Riverbend Labs, University of Georgia), and the total metal content, including iron and zinc, was determined to be less than 5% for all samples. Samples were then prepared in aqueous buffer (50 mM K-P_i, 200 mM NaCl, 143 mM β-ME, pH 6.5, or 150 mM Na_2SO_4, 100 mM Na-P_i, 143 mM β-ME, pH 7.0, containing 10% D_2O).

All NMR spectra were recorded on Varian Inova systems operating at either 499.678, 600.103, or 799.68 MHz proton frequency. Standard gradient-selected sensitivity-enhanced $^{1}H-^{15}N$ HSQC spectra used to monitor protein folding (*24*) were recorded with 2K direct points by 64 indirect points with sweep widths of 14−16 ppm in ^{1}H and 40 ppm in ^{15}N. Residual solvent was removed by convolution difference, and the data were apodized with a 90° shifted sine-bell window prior to Fourier transformation. NOESY and TOCSY data to be used in resonance assignment work were acquired as 2D homonuclear and ^{15}N-edited 2D and 3D versions. Similar data manipulations were performed as with the HSQC spectra.

Measurement of dipolar couplings requires that the protein be partially aligned in the magnetic field. This was ac-

complished using a suspension of filamentous bacteriophage (*19*, *25*). Phage Pf1 was made according to established protocols (*25*). Samples were then made by resuspending pelleted phage in the rubredoxin sample to a final concentration of 20−40 mg/mL of phage. The splitting of the deuterium resonance from the HOD in the buffer was determined and used as a measure of the degree of media orientation; splittings were typically in the range of 15−30 Hz. Paramagnetically aligned samples were measured at 500, 600, and 800 MHz using identical parameters at all three fields, and the expected B_0^2 field dependence was used to determine dipolar coupling contributions to resonance splittings (typically that of $^1H-^{15}N$ pairs).

Splittings were measured using the phase encoded HSQC-based experiment of Tolman and Prestegard (*26*). Briefly, this experiment is similar to the sensitivity enhanced HSQC, but instead of discarding components created by under- or overprecession during the internuclear transfer step, both in-phase and out-of-phase components are collected. After suitable manipulation, one matrix contains cross-peaks encoding the cosine-modulated signal and the other the sine-modulated signal. The sum of scalar and dipolar contributions ($J + D$) is then determined from volume ratios for each peak in the spectra according to the equation:

$$J + D = \frac{\arctan(\text{volume}_{\text{sine}}/\text{volume}_{\text{cosine}})}{(\pi \text{CT})} \qquad (1)$$

Here CT is the constant time period compensated for the presence of rf pulses (*26*). Separation of through-bond scalar components and through-space dipolar components that contribute to $^1H-^{15}N$ splittings requires that two measurements be taken: one for the protein in the isotropic phase and one for the protein in the aligned phase. Subtraction of the aligned from the isotropic values yields the residual dipolar coupling. All spectra were recorded on uniformly ^{15}N-labeled proteins between 3 and 10 mM. A constant time period of 43.01 ms ($4/J_{NH}$, $J_{NH} = 93$ Hz) was used for all spectra. Spectra were processed and volumes extracted using Felix (MSI). A Mathematica script was used to extract dipolar coupling values (Wolfram Research).

For more extreme conditions, inherent alignment at high magnetic field due to the large anisotropic magnetic susceptibility of the paramagnetic species was used. The specific conditions used were as follows: for CpFeRd, 0.1 and 0.5 M GuHCl at 25 and 45 °C, and for PfFeRd, 0.1, 0.5, 1, and 2 M GuHCl at 25 and 70 °C. These conditions were used to further explore the range over which these proteins remain folded.

Dipolar couplings were used primarily to test for consistency with known structures of the native forms. The dipolar couplings were analyzed using a variety of in-house software. First, these dipolar couplings are put through an order matrix analysis in conjunction with published crystal structures, as previously described (*21*, *22*). Residues which are in fast exchange or residues in highly mobile sections of the protein or which yield unreliable dipolar coupling values as the result of overlap were excluded from the order matrix analysis. Typically, 20−25 residues out of a potential 47 for the phage-aligned samples were used in the order matrix calculations, and 20 or more of 25 that could be seen in the paramagnetically aligned samples were used. Errors on dipolar couplings used in the order matrix calculations were typically 0.5 Hz for phage-aligned Zn samples, 0.5 Hz for field-aligned Fe samples, and 2 Hz for the phage-aligned apoproteins. A total of 10 000 cycles were used in each order matrix calculation. The solutions to the order parameters and Euler angles defining a principal order frame were then used to back-calculate dipolar couplings by manually reorienting the crystal structure to the order frame and using the program Dynamic (H. Valafar, available at http://tesla.ccrc.uga.edu). Predicted dipolar couplings were plotted versus the experimental dipolar couplings using a Mathematica script for presentation in correlation plots.

To validate our order matrix analysis and its subsequent use in creating these plots, we took one set of dipolar coupling data and performed several tests on it. In the first two tests we divided the data in half, picking every other point and determined an order tensor. This order tensor was then used to back-calculate all dipolar couplings. Comparison to scatter in plots using all data gives an assessment of how much choice of order parameters might hide changes in structures. No significant variations in the scatter were found. A last test was done to determine the level to which arbitrary data might accidentally be able to reproduce dipolar couplings. Dipolar couplings were scrambled randomly over structural sites, and the order matrix calculation was performed again. This resulted in no solutions under the conditions we used to determine the order tensor (10 000 cycles, 2 Hz error). Only when we used 100 000 cycles and an error of 5 Hz in the calculation did we obtain any solutions. Even under these extremely permissive conditions we only obtained 21 solutions for the order tensor. For comparison, normal order matrix analysis with 1 Hz errors and 10 000 cycles yields 2000 to 3000 solutions. Use of the order tensor from these scrambled data to back-calculate couplings also resulted in an experimental vs calculated plot that showed no significant correlation. Thus, our methodology seems capable of drawing reliable conclusions about variation in protein structure.

RESULTS

Even when principal order parameters and an alignment frame are adjusted to produce a best fit to experimental data, the scatter in back-calculated couplings is exquisitely sensitive to the assumed protein structure. If a correct structural model is used, a graph of experimental vs calculated couplings should show points falling on a diagonal line, except for scatter due to the error of the measurement. Any significant deviations from the line of unit slope result from motional averaging or true structural deviations. Figure 2 presents data on PfZnRd and CpZnRd at 25 °C where we expect a good correlation between experimental and back-calculated values. $^{15}N-^1H$ one-bond dipolar couplings range from −4 to +4 Hz spanning a range dependent on phage sample concentration but still reflecting the fundamental 3 $\cos^2\theta - 1$ dependence of couplings on overall N−H vector angles relative to the magnetic field. Order tensor solutions were determined using the dipolar data and the crystal coordinates of Bau et al. (*9*). Dipolar couplings were back-calculated from these values using a properly oriented structure. At 25 °C, neither PfZnRd nor CpZnRd shows systematic variations of measured dipolar couplings due to dynamics or changes in structure. The statistics of the fits,

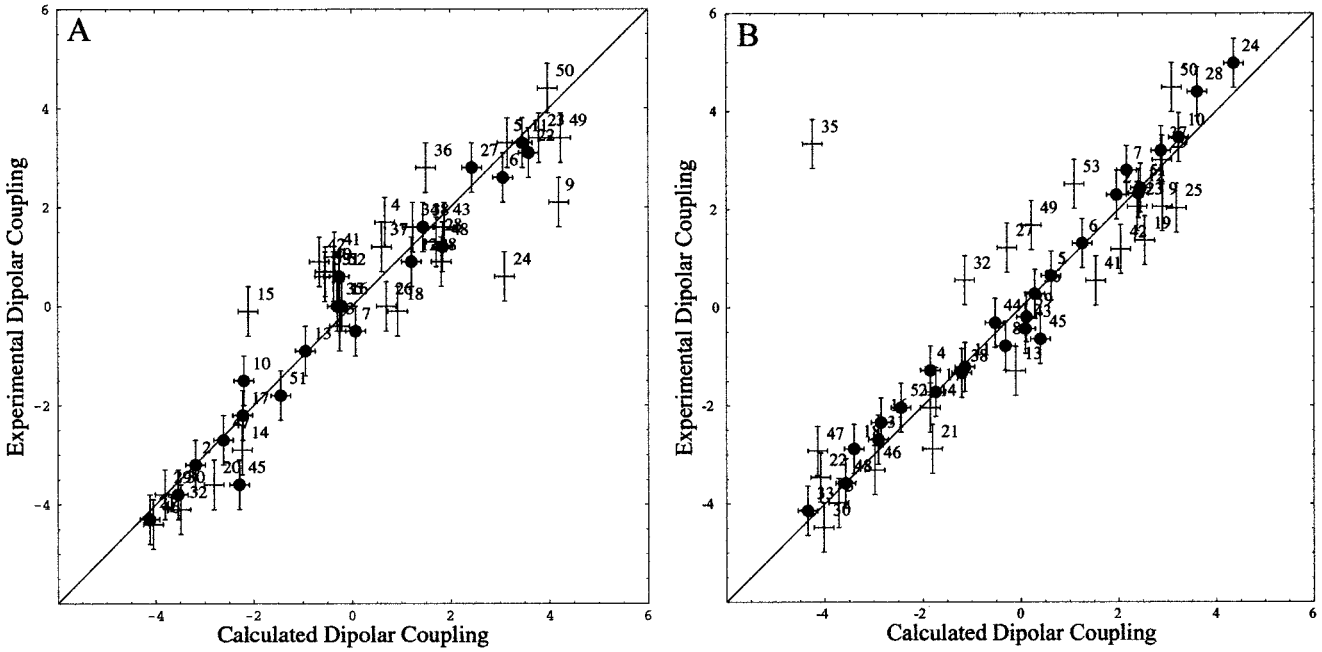

FIGURE 2: Plot of calculated vs experimental dipolar couplings for *P. furiosus* and *C. pasteurianum* zinc rubredoxin at 25 °C. (A) Data for PfZnRd using order tensor calculated with 20 of 47 residues and 0.5 Hz error. (B) Data for CpZnRd using order tensor calculated with 26 of 47 residues and 0.5 Hz error. Closed circles indicate those residues which were used in calculating the order tensor. Open circles indicate those residues which were not used in calculating the order tensor. The reason for their exclusion is discussed in the text.

Table 1: RMSD for Calculated vs Experimental Plots

sample conditions	RMSD in SVD (Hz)[a]	pts	RMSD for all (Hz)[b]	pts	pts > 2× error	r[c]
PfwtZnRd, 25 °C	0.49	20	0.64	42	5	0.97
PfwtZnRd, 70 °C	0.42	18	0.83	41	5	0.92
CpZnRd, 25 °C	0.42	26	0.66	43	4	0.97
CpZnRd, 70 °C	0.33	32	0.56	43	4	0.97
CpFeRd, 25 °C	0.19	21	0.21	24	0	0.95
CpFeRd, 45 °C, + 0.1 M GuHCl	0.23	21	0.22	23	1	0.53
apo-PfwtRd, 25 °C	0.95	29	1.55	34	5	0.96
apo-PfwtRd, 70 °C	0.98	26	1.18	29	5	0.97
apo-CpRd, 25 °C	2.61	17	2.57	19	0	0.57

[a] The RMSD for the points (pts) used in calculating the order tensor. [b] The RMSD for all points less than twice the error. [c] Correlation coefficient for all points less than twice the error.

including the RMSD of points from the best line, are given in Table 1. The deviations are somewhat larger than expected based on experimental precision, but they are no larger than variations that have been attributed to small variations in local bond lengths or N−H wagging in other protein structures. The plot of experimental vs calculated dipolar couplings at 25 °C demonstrates that the solution structure is the same as the crystal structure.

Upon heating to 70 °C, the continued correlation of calculated and measured dipolar couplings indicates that the structure of neither PfZnRd nor CpZnRd changes (Figure 3). The X-ray structure seems to model the solution structures well up to 70 °C. Since CpRd has a much shorter half-life at 100 °C ($t_{1/2}$ = 3 min vs 100 h for PfRd) (*12*), we might have expected to see structural changes associated with unfolding or large amplitude motions starting to manifest themselves in the residual dipolar coupling measurements of CpRd at 70 °C. For motion, we would expect a systematic reduction in the magnitude of measured couplings. If order tensor parameters from the 25 °C data were used in the back-calculation, this would result in a lower slope with points in less structured regions falling further off the line in the direction of lower magnitude. As can be seen in Figure 3, neither protein appears to have undergone structural changes or to show increased backbone motions at 70 °C. A best fit order tensor was used in the back-calculation (Figure 3), but principal parameters were only slightly lower than those from the 25 °C data; slightly lower alignment by phage is expected at 70 °C (∼20%). If the effects of phage-induced alignment are factored out, then the data for both proteins at 70 °C are very similar to the data acquired at 25 °C.

An attempt to destabilize the proteins using a combination of GuHCl and elevated temperatures was then made in order to further investigate structural changes that might occur prior to metal loss. Phage Pf1 is very susceptible to GuHCl denaturation and starts to lose its ability to act as an alignment medium at GuHCl concentrations as low as 0.1 M (data not shown). This eliminated phage as an option for an alignment medium. Instead, we used the inherent paramagnetic alignment of the iron form of Rd. This yields smaller residual dipolar coupling values (±1 Hz), but they can still be accurately determined using intensity-based methods for measuring couplings (*20*). As can be seen in Figure 4A, the CpFeRd at 25 °C gives measurements that can be reasonably well reproduced by back-calculation. Under mild denaturing conditions (0.1 M GuHCl and 45 °C) CpFeRd shows significant structural changes as evidenced by the scatter about the diagonal line (Figure 4B). However, the protein still maintains some sort of fold and is able to be oriented by the iron center (zero dipolar couplings would be expected for a random coil). PfFeRd, in contrast, showed no evidence of structural change even at 2 M GuHCl at 25 °C (data not shown). Only at 70 °C and 2 M GuHCl was a similar degree of destabilization observed as for CpFeRd at 45 °C and 0.1 M GuHCl (data not shown).

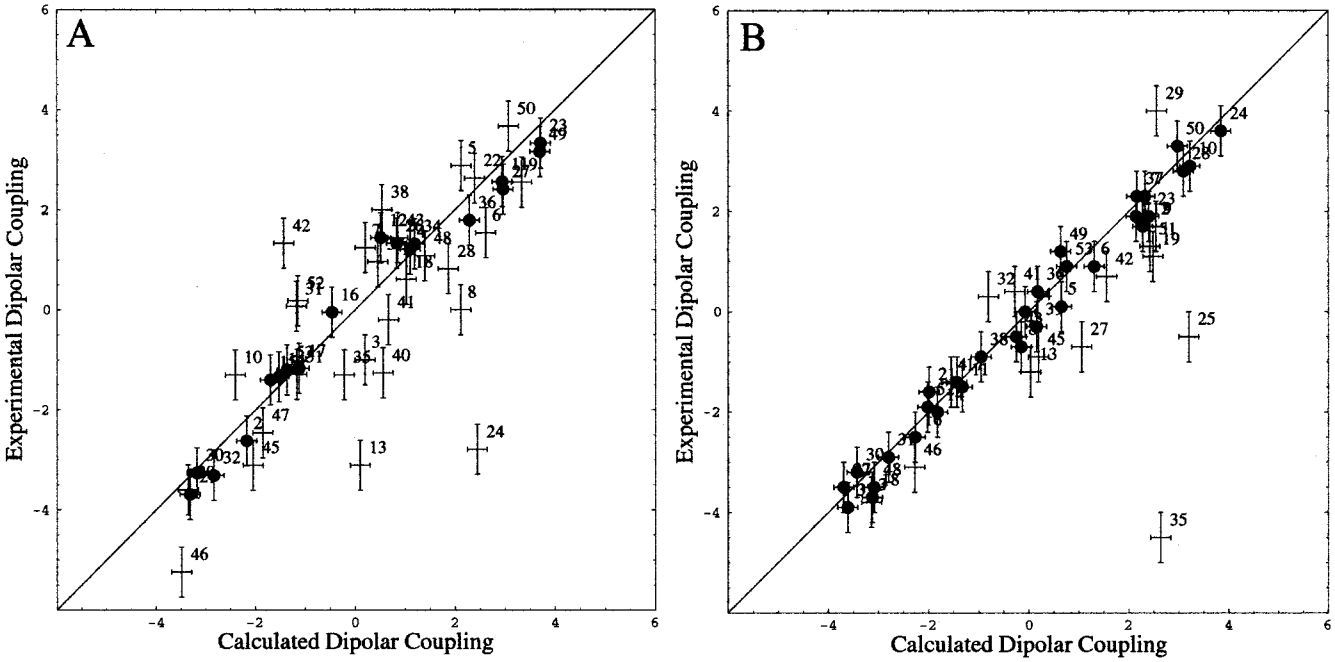

FIGURE 3: Plot of calculated vs experimental dipolar couplings for *P. furiosus* and *C. pasteurianum* zinc rubredoxin at 70 °C. (A) Data for PfZnRd using order tensor calculated with 18 of 46 residues and 0.5 Hz error. (B) Data for CpZnRd using order tensor calculated with 32 of 47 residues and 0.5 Hz error. Closed circles indicate those residues which were used in calculating the order tensor. Open circles indicate those residues which were not used in calculating the order tensor. The reason for their exclusion is discussed in the text.

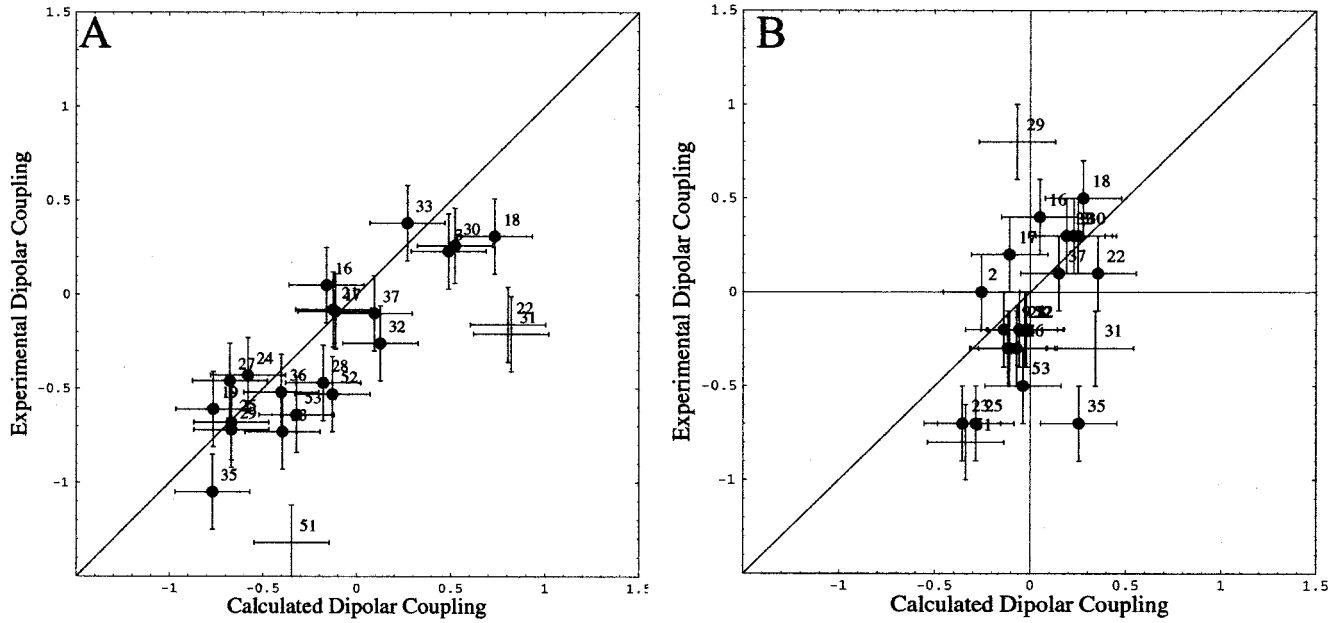

FIGURE 4: Plot of calculated vs experimental dipolar couplings for *C. pasteurianum* iron rubredoxin under native and destabilizing conditions. (A) Data for CpFeRd at 25 °C using order tensor calculated with 21 of 24 residues and 0.5 Hz error. (B) Data for CpFeRd at 45 °C with 0.1 M GuHCl using order tensor calculated with 21 of 47 residues. Closed circles indicate those residues which were used in calculating the order tensor. Open circles indicate those residues which were not used in calculating the 24 tensor. The reason for their exclusion is discussed in the text.

The apo forms of both rubredoxins were next investigated with the intent of passing reversibly from folded to unfolded forms. The fully folded state can be easily monitored through the characteristic chemical shift dispersion in an HSQC spectrum. On denaturation, the widely dispersed resonances characteristic of a folded protein disappear, and those more reminiscent of a random coil appear in the 7.8−8.6 ppm region in the proton dimension. Apo-PfRd appears to reach ∼50% unfolding at temperatures above 70 °C (Figure 5B). This unfolding was largely reversible upon returning the sample to 25 °C. The spectrum also shows a striking similarity to the native Zn form (Figure 5D). Assignments for most of the amides in apo-PfRd were mapped from the HSQC of the native form and verified using TOCSY and NOESY experiments. The largest deviations in cross-peak position were, as expected, associated with residues near the metal site (a table of assignments is given in the Supporting Information).

Apo-CpRd was then observed before and after heating to 70 °C. As seen in Figure 6A, it is folded and maintains

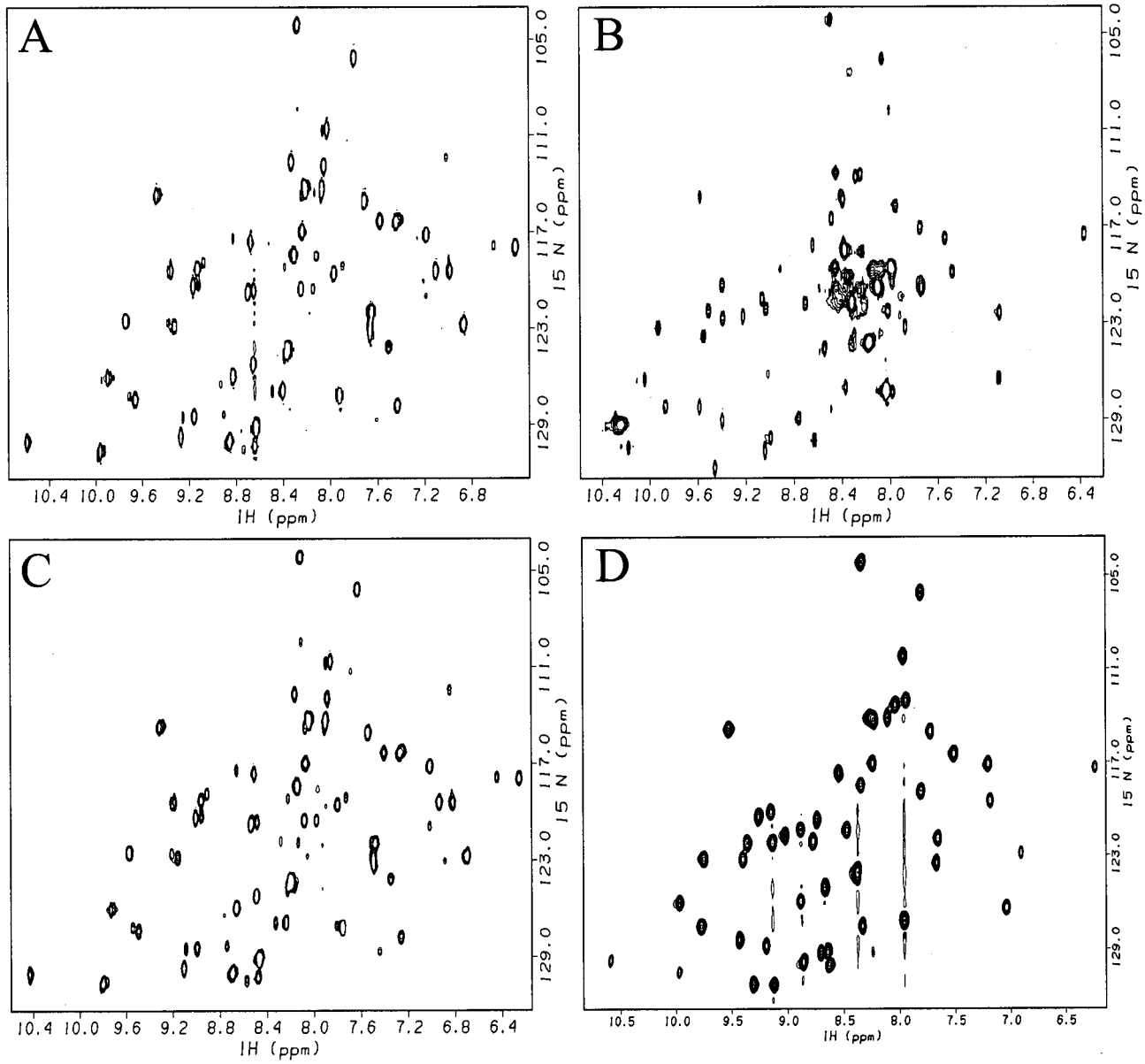

FIGURE 5: HSQC spectra of PfZnRd and apo-PfRd. (A) $^{1}H-^{15}N$ HSQC of apo-PfRd at 25 °C. (B) $^{1}H-^{15}N$ HSQC of apo-PfRd at 70 °C. (C) $^{1}H-^{15}N$ HSQC of apo-PfRd at 25 °C immediately after being at 70 °C. (D) $^{1}H-^{15}N$ HSQC of PfZnRd at 25 °C shown for reference. All spectra are displayed in order to have comparable intensities to allow direct comparison.

secondary structure at 25 °C as indicated by the HSQC chemical shift dispersion. However, there is much less similarity to the native form (Figure 6D). Only a few assignments could be determined directly by resonance mapping between the native and apo form. However, TOCSY/NOESY methodology was able to assign additional peaks; 23 unambiguous assignments for apo-CpRd were obtained (Supporting Information). Upon raising the temperature, the apo-CpRd is completely unfolded at 70 °C; even at the relatively low temperature of 40 °C, the protein is about 50% unfolded. This unfolding process is at least partially reversible upon return to low temperature.

Dipolar couplings were measured on the apo form of PfRd at 25 and 70 °C and on apo-CpRd at 25 °C to corroborate the suggested similarity and dissimilarity of the demetalated forms. Amazingly, there were few large amplitude deviations from the predicted dipolar couplings based on the structure of the native metalated protein in apo-PfRd at either 25 °C or for the remaining folded component at 70 °C. (Figure 7). In agreement with suggestions made on the basis of similarity in HSQC cross-peak positions, this indicates that the apo and native states of PfRd have very similar structures. The magnitudes of the couplings at 70 °C are only attenuated by the lower degree of order imparted by the phage at this temperature. There are a few additional residues that are not calculated accurately in apo-PfRd. On the basis of our inability to provide assignments for these residues it appears that these residues are those near the metal binding site (Pf residues 6−10 and 38−41 and Cp residues 3−11 and 36−45). Many of these residues are also doubled, indicating a slow equilibration among conformational states for these residues.

Residual dipolar coupling measurements on apo-CpRd yielded very interesting results. Despite its lower thermostability and structural changes, apo-CpRd is still structured enough at 25 °C to be aligned and have dipolar couplings measured from it. If the protein had the disorder of a true random coil, internal motions would reduce all dipolar

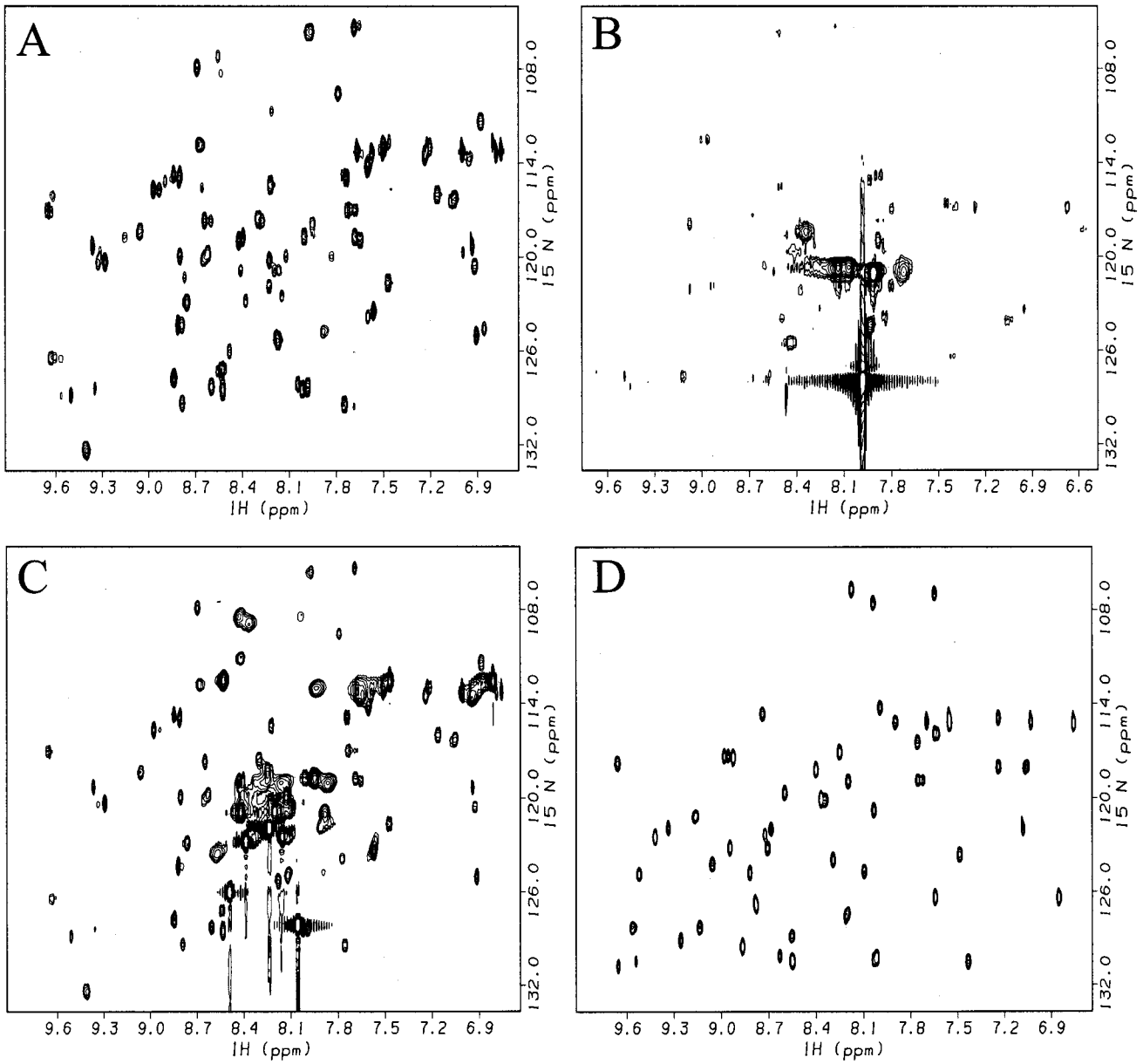

FIGURE 6: HSQC spectra of CpZnRd and apo-CpRd. (A) $^{1}H-^{15}N$ HSQC of apo-CpRd at 25 °C. (B) $^{1}H-^{15}N$ HSQC of apo-CpRd at 70 °C. (C) $^{1}H-^{15}N$ HSQC of apo-CpRd at 25 °C immediately after being at 70 °C. (D) $^{1}H-^{15}N$ HSQC of CpZnRd at 25 °C shown for reference. All spectra are displayed in order to have comparable intensities to allow direct comparison.

couplings to near zero. Using the crystal structure of the native CpFeRd and the order tensor determined by order matrix analysis (using the same errors as for the apo-PfRd, 2.0 Hz), the dipolar couplings for apo-CpRd were back-calculated (Figure 8). Clearly, there are significant structural changes in the protein. This supports the suggested change based upon chemical shift alterations in the HSQC spectrum.

A large number of variants exist for both Pf and Cp rubredoxin; in addition, chimeras exist for both proteins (*14*). Comparison of the apo form of two of these variants offers an opportunity to focus on possible origins of thermodynamic stability. The first variant is PfRd with three point mutations,-W3Y/I23V/L32I. This changes the hydrophobic core of PfRd to match that of CpRd. The other is a chimera that has the first 15 residues of CpRd followed by the remaining 38 residues of PfRd. The first 15 residues encompass the first two strands of the β-sheet of rubredoxin which contain one-half of the metal binding site and the key residue, E15, in the PfRd hydrogen-bonding network. The apo-PfRd with the Cp hydrophobic core exhibits similar stability (perhaps even greater stability) to the parent PfRd, maintaining the tertiary fold up to 70 °C with only slight unfolding (Figure 9). This suggests that differences in the hydrophobic core are not a major determinant of hyperthermostability. The apo chimera of PfRd with the first 15 residues of CpRd did not exhibit the stability of apo-PfRd. At 25 °C, it already shows excess cross-peak intensity in the random coil region. It was almost completely unfolded at 70 °C (Figure 10). Also, unlike the other three proteins studied, this unfolding was not reversible. Hence, the unusual structural stability of PfRd may derive in part from interactions involving the first 15 residues.

DISCUSSION

Biochemical studies clearly show that the native state of CpRd is less stable kinetically than PfRd above 70 °C, yet it appears to maintain a native structure at 70 °C (Figures 2

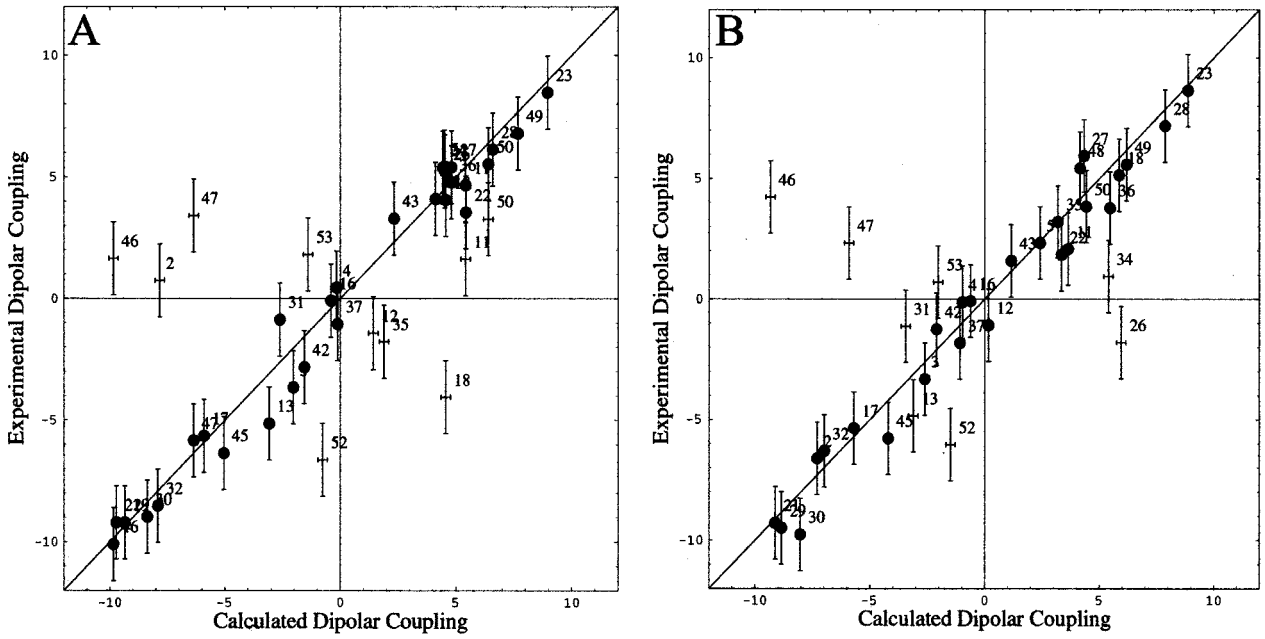

FIGURE 7: Plot of calculated vs experimental dipolar couplings for *P. furiosus* apo-Rd. (A) Data for apo-PfRd at 25 °C using order tensor calculated with 29 of 39 residues and 2 Hz error. (B) Data for apo-PfRd at 70 °C using order tensor calculated with 26 of 34 residues. Closed circles indicate those residues which were used in calculating the order tensor. Open circles indicate those residues which were not used in calculating the order tensor. The reason for their exclusion is discussed in the text.

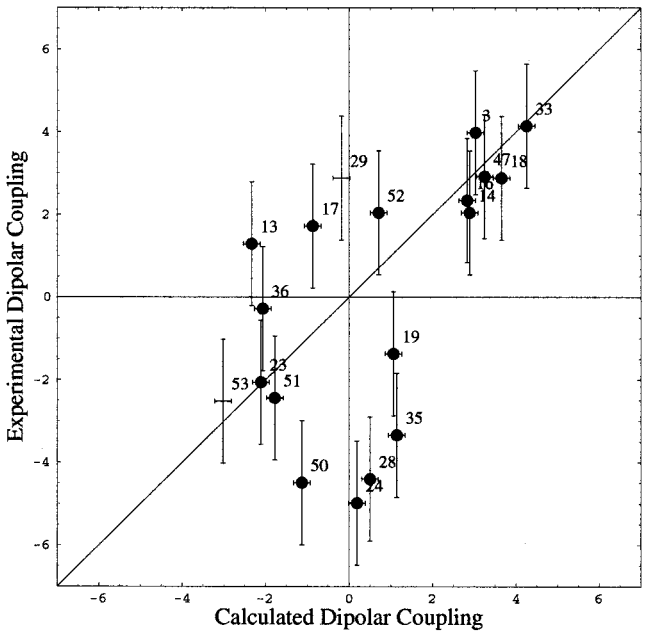

FIGURE 8: Plot of calculated vs experimental dipolar couplings for *C. pasteurianum* apo-Rd. (A) Data for apo-CpRd at 25 °C using order tensor calculated with 29 of 39 residues and 2 Hz error. (B) Data for apo-CpRd at 70 °C using order tensor calculated with 26 of 34 residues. Closed circles indicate those residues which were used in calculating the order tensor. Open circles indicate those residues which were not used in calculating the order tensor. The reason for their exclusion is discussed in the text.

and 3). Neither protein exhibits significant deviations of measured residual dipolar couplings from those predicted on the basis of the native structure; these would be expected if the proteins were undergoing large amplitude backbone motions or conformational changes as a preliminary step toward metal loss.

There do, however, appear to be differences in stability of metalated PfRd and CpRd when subjected to harsh conditions. Whereas PfFeRd required 2 M GuHCl and 70 °C to become destabilized, much milder conditions were required in CpFeRd (0.1 M GuHCl and 45 °C). In both cases, the metal binding sites seem to remain intact as the proteins were able to be aligned enough through the anisotropic magnetic susceptibility of the paramagnetic center in the presence of a strong magnetic field. There is a slightly lower range of couplings under the harsher conditions (~30%). While we cannot exclude a reduction in the anisotropic susceptibility of the metal site, a reduction in range is consistent with a higher degree of internal motion. The effects of destabilization that we observe as departures from our calculated dipolar couplings seem, therefore, not to be associated with the kinetic step of iron loss. Instead, this destabilization seems to arise from some property of the underlying protein structure.

Suggestions that thermophilic and mesophilic proteins would differ in terms of flexibility of their structural cores have persisted for some time (*27*). Underlying this suggestion is the observation that maximum efficiency of enzyme-catalyzed reactions often occurs at higher temperatures for proteins from hyperthermophiles; this is rationalized in terms of higher temperatures being needed to allow catalytic motions in more rigid hyperthermophilic proteins. That we cannot detect differences between rubredoxins from a mesophile and a hyperthermophile at 70 °C without added denaturants may simply reflect that differences in amplitudes of motion under these conditions are too small to be reflected in our residual dipolar coupling measurements or that differences are largely relegated to side chain motions which we cannot directly detect. Changes in the structure of CpRd that allow increased association of ANS, a probe of hydrophobic accessibility, have been observed at temperatures as low as 60 °C (*28*). It is possible that this is again more directly a function of side chain rearrangement. Amide exchange rates, which do more directly reflect backbone

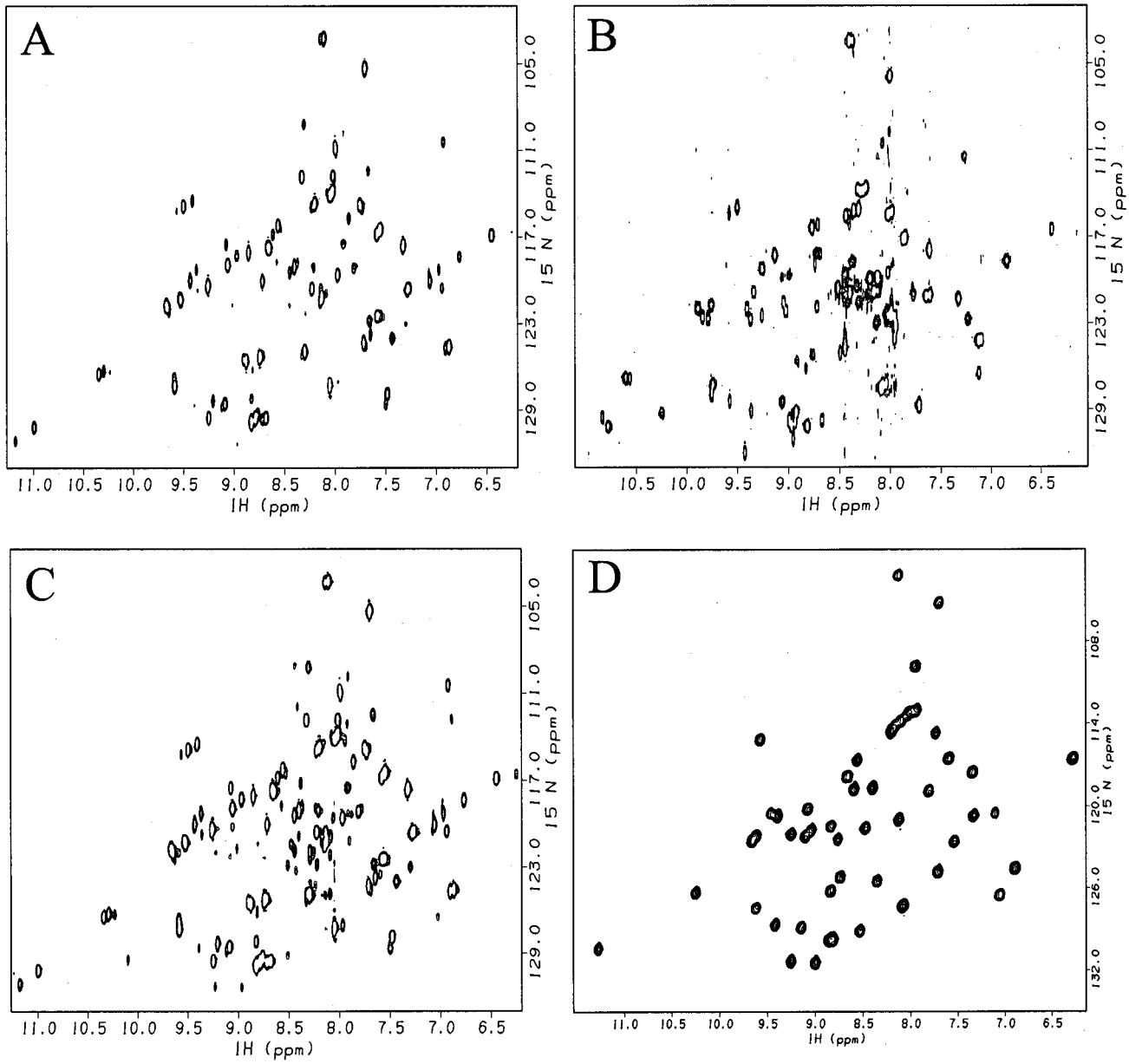

FIGURE 9: HSQC spectra of PfZnRd(W3Y/I23V/L32I) and apo-PfRd(W3Y/I23V/L32I). (A) $^{1}H-^{15}N$ HSQC of apo-PfRd(W3Y/I23V/L32I) at 25 °C. (B) $^{1}H-^{15}N$ HSQC of apo-PfRd(W3Y/I23V/L32I) at 70 °C. (C) $^{1}H-^{15}N$ HSQC of apo-PfRd(W3Y/I23V/L32I) at 25 °C immediately after being at 70 °C. (D) $^{1}H-^{15}N$ HSQC of PfZnRd(W3Y/I23V/L32I) at 25 °C shown for reference. All spectra are displayed in order to have comparable intensities to allow direct comparison.

properties, do not indicate any unusual rigidity for the PfRd backbone, at least at the moderate temperatures and rather high pH of a recent study (*29*). Our observation that denaturants in combination with temperature can lead to differences in backbone structure and dynamics suggests that differences may exist at higher temperatures. As these temperatures are not accessible with our current NMR probes, and as differences appear to be uncorrelated with metal loss, an examination of the properties of the apoproteins appears to be a good alternative to direct observation on the metalated proteins.

Both residual dipolar coupling data and the similarity of cross-peak positions in the HSQC spectra indicate that the structures of apo-PfRd and native PfZnRd are remarkably similar. The agreement of measured couplings of apo-PfRd with those back-calculated using the metalated PfRd structure means that the structure of apo-PfRd, except in and near the metal binding site, is very nearly the same as the native PfRd, even up to 70 °C. The peaks which are not accurately back-calculated include the ones in PfZnRd that seem to originate from rapid amide exchange, overlap, and conformational flexibility, but additional ones near the metal binding site are now included in this set. Although many apoproteins retain a native or near native structure, they are usually larger than rubredoxin (*30*). It is unusual for a 53-residue apoprotein to be structured and to retain the three-dimensional structure of the native state. The extreme stability of the apo-PfRd structure emphasizes the lack of a role for the metal in thermostability.

Unlike apo-PfRd, the HSQC of apo-CpRd even at 25 °C was markedly different from the spectrum of the native CpZnRd. There is still good chemical shift dispersion at this low temperature, and the peaks are narrow; however, the peaks have shifted considerably (Figure 6). When the native

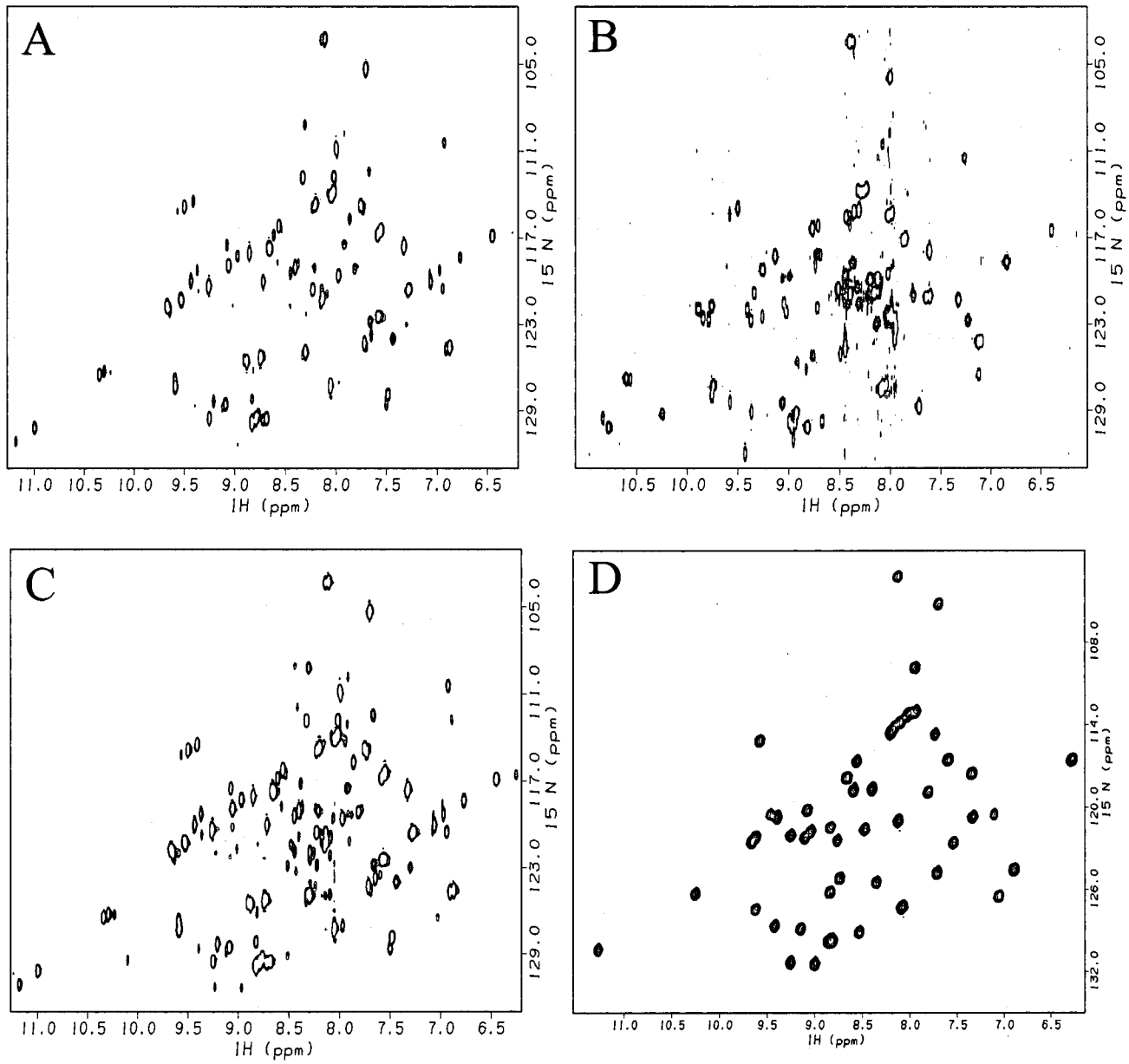

FIGURE 10: HSQC spectra of ZnCp15Pf and apo-Cp15Pf. (A) $^{1}H-^{15}N$ HSQC of apo-Cp15Pf at 25 °C. (B) $^{1}H-^{15}N$ HSQC of apo-Cp15Pf at 70 °C. (C) $^{1}H-^{15}N$ HSQC of apo-Cp15Pf at 25 °C immediately after being at 70 °C. (D) $^{1}H-^{15}N$ HSQC of ZnCp15Pf at 25 °C shown for reference. All spectra are displayed in order to have comparable intensities to allow direct comparison.

crystal structure was used to calculate the dipolar couplings for apo-CpRd, it became readily apparent that the structure was completely different from the native state. Hence, CpRd undergoes some structural change upon metal loss, in direct contrast to PfRd, which does not. Apo-CpRd was also far less thermostable than apo-PfRd, rapidly unfolding as the temperature was increased. Its approximate T_m of 40 °C is half that of the engineered metal-free Rd (*15*) and of apo-PfRd. We have not attempted to determine the structure of apo-CpRd at this point, but it will be the basis of a future more detailed study.

A number of characteristics of the underlying protein structure have been suggested to dictate thermostability. For example, increased packing density, increased core hydrophobicity, decreased length of surface loops, improved secondary structure, capping, salt bridges, and hydrogen bonds have all been suggested. So far, however, no single determinant of thermostability for rubredoxin has been identified. This is in contrast to a similarly sized protein (67 residues) from *Bacillus caldolyticus* where two surface amino acids were shown to contribute up to 70% of the thermostability of the protein (*31*). Two possible contributors to the stability of the apo state can be evaluated from the results on chimeras, contributions from the hydrophobic core and from hydrogen bonds/ion pairs. The hydrophobic core in PfRd is composed of eight residues: W3, Y10, Y12, I23, F29, L32, W36, and F48. The hydrophobic core of PfRd can be changed to match that of CpRd with only three mutations, W3Y, I23V, and L32I. This core mutant is as kinetically stable as the parent PfRd at neutral pH (F. E. Jenney, Jr., personal communication), suggesting that the PfRd core does not make a unique contribution to stability. Our HSQC-based results extend the kinetic similarity of the mutant and native protein to the thermodynamic stability of the apo form (Figure 9).

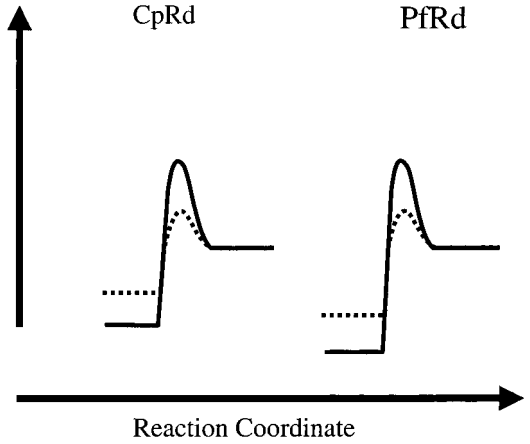

FIGURE 11: Thermodynamic model for the origin of hyperthermostability. The dotted lines indicate the free energy for the apo state, and the solid lines indicate the free energy for the native, metalated protein.

The rubredoxin chimera Cp15Pf (*14*) has the first two strands of the β-sheet of CpRd combined with the last 38 residues of PfRd. The strands of the β-sheet encompass half of the metal binding site, a network of hydrogen bonds, and two salt bridges. The possible importance of hydrogen bonds and ion pairs in the N-terminal segment for improving stability has been suggested previously (*7*). Remarkably, the chimera is kinetically destabilized even relative to CpRd ($t_{1/2}$ of 3.6 h vs 5.8 h for CpRd at 92 °C) (*14*). Our HSQC-based results support an important role for the first 15 residues in stability but assign that role to the thermodynamic stability of the underlying protein framework. In contrast to the native apo-PfRD when the temperature is raised to 70 °C, the chimera is almost completely unfolded.

We propose a simple thermodynamic model that can fit the available data. In this model (Figure 11), the thermodynamic difference in the two rubredoxins arises solely from differences in the protein structure. Specifically, the free energy of the native state is lower for the hyperthermophilic than the mesophilic rubredoxin. The metal has no differential effect; it contributes equally to the stability of both proteins. The difference in kinetic stability could arise strictly from the higher activation energy that results from the lower free energy of the apo-PfRd. The specific property of the protein that leads to this difference is not known with certainty at this point, but our results clearly point to the hydrogen-bonding network or other interactions involving these first 15 residues.

Recently, forms of PfRd lacking the metal binding site have been engineered to selectively remove ion pairs involving residues in the N-terminal segment (*32*). The only significant contributor to stability of the PfRd appears to be the ion pair from the N-terminal amino group to the side chain carboxyl of Glu14. CpRd, including the Cp15Pf construct used here, has the glutamic acid displaced to position 15 as well as an N-terminal Met that displaces the N-terminal amino group. Hence, the absence of an ion pair could contribute to the destabilization of the Cp15Pf construct. Recently, the crystal structure of the chimeric Rd Cp15Pf has also been solved (C.-H. Kang, Washington State University, personal communication). There is a steric clash between residue Cp2K and Pf50K, and this clash could also be the source of some destabilization. As to possible contributions due to differences in the strength and extent of a hydrogen-bonding network, new NMR techniques that can directly probe hydrogen bonding offer an interesting route to further differentiation of these possible explanations (*33*−*35*).

ACKNOWLEDGMENT

We thank H. al-Hashimi, A. Fowler, F. Tian, and M. Fischer for very helpful discussions regarding the obtaining and analysis of dipolar couplings.

SUPPORTING INFORMATION AVAILABLE

Tables of assignments for the apo-PfRd and apo-CpRd. This material is available free of charge via the Internet at http://pubs.acs.org.

REFERENCES

1. Lowery, M. D., Guckert, J. A., Gebhard, M. S., and Solomon, E. I. (1993) *J. Am. Chem. Soc. 115*, 3012−3013.
2. Bennet, D. E., and Johnson, M. K. (1987) *Biochim. Biophys. Acta 911*, 71−80.
3. Wilkens, S. J., Xia, B., Weinhold, F., Markley, J. L., and Westler, W. M. (1998) *J. Am. Chem. Soc. 120*, 4806−4814.
4. Ayhan, M., Xiao, Z., Lavery, M. J., Hamer, A. M., Nugent, K. W., Scrofani, S. D. B., Guss, M., and Wedd, A. G. (1996) *Inorg. Chem. 35*, 5902−5911.
5. Kummerle, R., Zhuang-Jackson, H., Gaillard, J., and Moulis, J.-M. (1997) *Biochemistry 36*, 15983−15991.
6. Stalhandske, C. M. V., Dong, J., Tavares, P., Liu, M.-Y., LeGall, J., Moura, J. J. G., Moura, I., Park, J.-B., Adam, M. W. W., and Scott, R. A. (1998) *Inorg. Chim. Acta 273*, 409−411.
7. Blake, P. R., Park, J. B., Zhou, Z. H., Hare, D. R., Adams, M. W. W., and Summers, M. F. (1992) *Protein Sci. 1*, 1508−1521.
8. Blake, P. R., Day, M. W., Hsu, B. T., Joshua-Tor, L., Park, J. B., Hare, D. R., Adams, M. W., Rees, D. C., and Summers, M. F. (1992) *Protein Sci. 1*, 1522−1525.
9. Bau, R., Rees, D. C., Kurtz, D. M., Jr., Scott, R. A., Huang, H., Adams, M. W. W., and Eidsness, M. K. (1998) *J. Biol. Inorg. Chem. 3*, 484−493.
10. Dauter, Z., Wilson, K. S., Sieker, L. C., Moulis, J.-M., and Meyer, J. (1996) *Proc. Natl. Acad. Sci. U.S.A. 93*, 8836−8840.
11. Cavagnero, S., Zhou, Z. H., Adams, M. W., and Chan, S. I. (1995) *Biochemistry 34*, 9865−9873.
12. Cavagnero, S., Zhou, Z. H., Adams, M. W., and Chan, S. I. (1998) *Biochemistry 37*, 3377−3385.
13. Cavagnero, S., Debe, D. A., Zhou, Z. H., Adams, M. W. W., and Chan, S. I. (1998) *Biochemistry 37*, 3369−3376.
14. Eidsness, M. K., Richie, K. A., Burden, A. E., Kurtz, D. M., Jr., and Scott, R. A. (1997) *Biochemistry 36*, 10406−10413.
15. Strop, P., and Mayo, S. L. (1999) *J. Am. Chem. Soc. 121*, 2341−2345.
16. Strop, P., and Mayo, S. L. (2000) *Biochemistry 39*, 1251−1255.
17. Hiller, R., Zhou, Z. H., Adams, M. W. W., and Englander, S. W. (1997) *Proc. Natl. Acad. Sci. U.S.A. 94*, 11329−11332.
18. Tjandra, N., and Bax, A. (1997) *Science 278*, 1111−1113.
19. Hansen, M. R., Mueller, L., and Pardi, A. (1998) *Nat. Struct. Biol. 5*, 1065−1074.
20. Tolman, J. R., Flanagan, J. M., Kennedy, M. A., and Prestegard, J. H. (1995) *Proc. Natl. Acad. Sci. U.S.A. 92*, 9279−9283.
21. Fischer, M. W. F., Losonczi, J. A., Weaver, J. L., and Prestegard, J. H. (1999) *Biochemistry 38*, 9013−9022.

22. Losonzci, J. A., Andrec, M., Fischer, M. W. F., and Prestegard, J. H. (1999) *J. Magn. Reson. 138*, 334−342.
23. Blake, P. R., Park, J. B., Bryant, F. O., Aono, S., Magnuson, J. K., Eccleston, E., Howard, J. B., Summers, M. F., and Adams, M. W. (1991) *Biochemistry 30*, 10885−10895.
24. Palmer, A. G. I., Cavanagh, J., Byrd, R. A., and Rance, M. (1992) *J. Magn. Reson. 96*, 416−424.
25. Hansen, M. R., Hanson, P., and Pardi, A. (2000) *Methods Enzymol. 317*, 220−240.
26. Tolman, J. R., and Prestegard, J. H. (1996) *J. Magn. Reson., Ser. B 112*, 245−252.
27. Jaenicke, R. (2000) *Proc. Natl. Acad. Sci. U.S.A. 97*, 2962−2964.
28. Bonomi, F., Fessas, D., Iametti, S., Kurtz, D. M., Jr., and Mazzini, S. (2000) *Protein Sci. 9*, 2413−2426.
29. Hernandez, G., Jenney, F. E., Jr., Adams, M. W. W., and LeMaster, D. M. (2000) *Proc. Natl. Acad. Sci. U.S.A. 97*, 3166−3170.
30. Spolar, R. S., and Record, M. T. J. (1994) *Science 263*, 777−784.
31. Perl, D., Mueller, U., Heinemann, U., and Schmid, F. X. (2000) *Nat. Struct. Biol. 7*, 380−383.
32. Strop, P., and Mayo, S. L. (2000) *Biochemistry 39*, 1251−1255.
33. Cordier, F., and Grzesiek, S. (1999) *J. Am. Chem. Soc. 121*, 1601−1602.
34. Meissner, A., and Sorenson, O. W. (2000) *J. Magn. Reson. 143*, 387−390.
35. Meissner, A., and Sorenson, O. W. (2000) *J. Magn. Reson. 143*, 431−434.

BI0026831